M. Chaieb
S. Tounsi,
R. Neji

J. Electrical Systems 5-1 (2009):

Regular paper

Design and optimization of axial permanent magnet machine for electric vehicle

The application of permanent magnet in electrical machines increases their efficiency by eliminating the excitation losses, which means a higher output power or torque per volume than when using electromagnetic excitation. In this paper, a drive system based on a modular structure of permanent magnet machine is proposed. The main objective is to conceive an actuator having a high starting torque, height specific power and high efficiency. Modular structure offers the possibility of power augmentation by insertion of modules. This characteristic reduces significantly the manufacturing cost. Machine structure and the proposed 2-D model are presented in the first part. The second section introduces the sizing approach using generalized sizing equations. The initial calculation of motor dimensions and parameters, namely, the electric constant, slots height, permanent magnet size, and coil turns, are also presented. In the third part finite elements analysis of the structures is investigated to get an insight of field distribution, flux directions and paths in different parts of the machines for different load conditions. Furthermore, torque and cogging torque of the machine are analysed by using of finite elements method to validate analytic approach.

KEYWORDS: Permanent Magnet motor, finite elements method, optimization, design, electric vehicle.

1. Introduction

In a world where environmental protection and energy conservation are of growing concerns, the development of electric vehicle technology has taken an accelerated pace to fulfil these needs. Concerning the environment, electric Vehicles can provide emission-free urban transportation.

In this context, Permanent magnet synchronous motors gain more and more importance for special drive applications [1]. Up to recent years, Permanent magnet synchronous motors were known for small drives, e.g. for servo applications. Development in the last years extended the motor ratings up into the MW-range. Today such large capacity Permanent magnet motors are applied in high speed drives as well as in low speed drives.

High torque density and high efficiency are two of the most desirable features for an electrical machine. Improvement of these performances has been one of the main aspects of research on the electric machines. Several new topologies [2,3] have been proposed and improved torque density or efficiency was reported.

Axial flux permanent magnet synchronous machines have been studied with increasing interest, mainly because the permanent magnet machine structure and performance fit very well into the requirements of the electrical vehicles motors (low-speed, high-torque) [4,5]. These machines have several unique features such as high efficiency, high specific power and torque densities, low rotor losses and small magnetic thickness.

Axial flux permanent magnet machine types are basically different combinations of various features which can be classified as:

A. Stator-rotor arrangement:

- Multi-disk structure.
- Single-sided structure (Fig 1).

Laboratory of Electronic and Information Technology -LETI- Equip of Electric Vehicle and Power Electronics - VEEP- National Engineering School B.P.: W, 3038 Sfax-Tunisia

- Double-sided structure.
    - Internal rotor (Fig 2).
    - Internal stator (Fig 3).

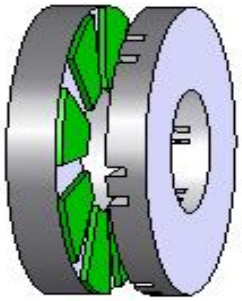

Figure1: Single-sided structure

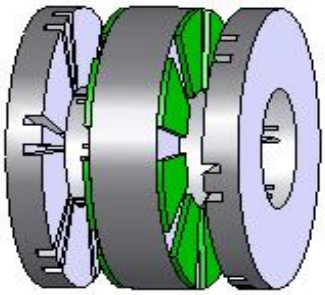

Figure2: Double-sided structure (Internal rotor)

B. The technique to integrate the permanent magnets to the rotor:

- Surface-mounted permanent magnet type.
- Internal or buried permanent magnet type.

2. Machine Structure

The machine has one stator and two rotors. The stator has a slotted structure with double face. The rotors structure is formed by two discs, surface mounted permanent magnets and a shaft. The two rotors carry the axially magnetized magnets which are mounted on the inner surfaces of the two rotor discs.

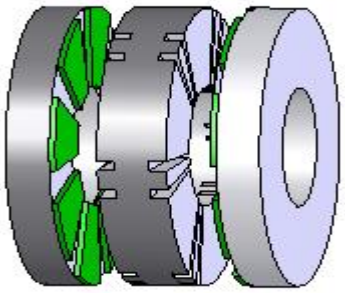

Figure 3: Double-sided structure (Internal stator)

Each rotor and a stator surface are composed of eight magnets, six main teeth with a concentrated winding and six inserted teeth so as to reduce the leakage flux and to improve the electromotive force wave form and twelve slots.

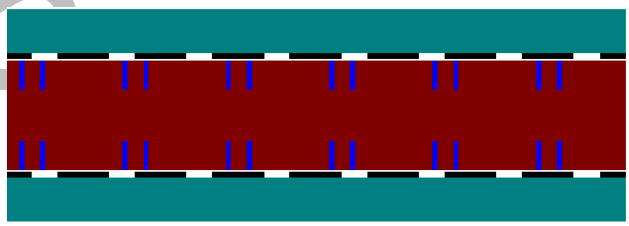

Figure 4: 2D-model of axial flux permanent magnet machine

3. Analytical Dimensioning

A. Student configuration

¶The configuration of the motor is characterized by a relation ship between the number of teeth and the number of poles pairs directly bound to the space percentage occupied by the slots compared to that occupied by the inserted tooth.¶ ¶Three design ratios define the motor's structure:¶

Four configurations with sinusoidal wave-form that respect these rules are found. Each of them is characterised by a law of the variation of the pairs pole number (p) in function of un integer (n) varying from one to infinity, a ratio (r) of the principal teeth number N_d by the pairs pole number (p) and the ratio (ν) of the free space between two principal teeth by the space occupied by one principal tooth. The following table gives three ratios for each configuration [6].

TABLE 1: Motor configurations

Sinusoidal configurations	P	r	ν	α	β
1	2.n	1.5	1	2/3	1
2	5.n	1.2	3/2	2/3	1
3	2.n	1.5	1/3	3/2	2/3
4	5.n	1.2	2/3	3/2	2/3

with:

- β is the magnet angular width by the pole pitch,
- α is the main tooth angular width by the magnet angular.

B. the motor sizing

Relationships between input and output parameters are established by analytic equations that translate fundamental principles of the electromagnetism.

In figure 5 the outside and inside diameters of the stator (D_{int} and D_{ext}), and the effective length of the stator core in radial direction $(D_{ext} - D_{int})$ are shown.

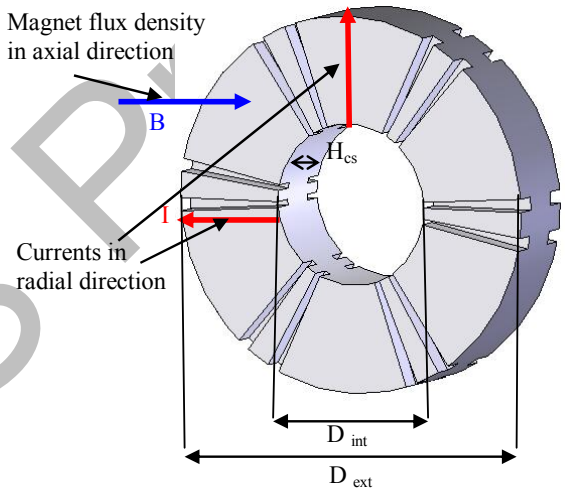

Figure 5: Stator structure

The emf induced in the stator windings from the rotor excitation system can be expressed. As it is seen from figure 5, the rotor excitation system rotates with velocity v

with respect to the stator conductors which are perpendicular to the direction of the magnetic field.

The amplitude of the emf is mainly fixed by the air-gap induction. The emf obtained in the winding are deduced from the flux derivative. It is necessary to be able to express the flux in function of magnets position. In this approach, the variation of the common area between a main tooth and a magnet is supposed to be linear in function of the rotor rotation.

The maximal value of emf derive from flux calculation is expressed as follows [7,8]

$$E = \frac{N_{sph}\left(D_{ext}^2 - D_{int}^2\right)B_e\,\Omega}{4} \tag{1}$$

with:

- Ω is the angular velocity of the motor,
- N_{sph} is the number of spire by phase.

For a food with current of maximum amplitude I and in phase with the back emf, the electromagnetic torque developed by the motor takes the following form [9]:

$$T_m = \frac{3}{2}\frac{EI}{\Omega} \tag{2}$$

The electric constant of the motor is defined by:

$$K_e = \frac{3}{2} N_{sph}\left(D_{ext}^2 - D_{int}^2\right)B_e \tag{3}$$

The maximum value of the back emf takes the following form:

$$E = \frac{2}{3} K_e\,\Omega \tag{4}$$

The electromagnetic torque becomes:

$$T_m = K_e\, I \tag{5}$$

The axial motor parameters are computed as previously thanks to basic electromagnetism laws. Contrary to radial machines, there are no height constraints for these parameters. For example, the slot height is chosen in function of admissible current density and filling factor, it is independent of the airgap volume [10].

The magnet thickness fixes the induction level in the airgap. This parameter is given by applying the Ampere Law when a magnet overlays a main tooth. The flux created by magnets is composed of the leakage flux between magnets and the useful flux crossed stator [11].

The expression gives the slots height in function of the current density and the available surface:

$$H_e = \frac{3.2\, N_{sph}}{2\, N_d}\frac{I}{\sqrt{2}\,\delta}\frac{1}{K_r\, L_{enc}} \tag{6}$$

with:

- N_d is the main teeth number,
- δ is the current density in slots,
- K_r is the filling coefficient of slots,
- L_{enc} is the slots width.

The magnet width is:

$$E_a = \mu_r \frac{B_e}{B_r - \frac{B_e}{K_{fu}}} e \quad (7)$$

with:

- μ_r is the magnet relative permeability,
- B_r is the remanence,
- K_{fu} is the coefficient of flux leakages,
- e is the air-gap thickness.

To avoid the demagnetization, the current of phase must be below I_d:

$$I_d = \left(\frac{B_r - B_c}{\mu_r} E_a - B_c K_{fu} e \right) \frac{2p}{\mu_0} \quad (8)$$

with:

- B_r is the minimum flux density allowed in the magnets,
- B_c is the demagnetization induction,
- μ_0 is the permeability of the air.

The yoke rotor thickness H_{cr} and the yoke stator thickness H_{cs} are obtained from the flux conservation law [12]:

$$H_{cr} = \frac{B_e}{B_{cr}} \frac{S_d}{(D_{ext} - D_{int})} \frac{1}{K_{fu}} \quad (9)$$

$$H_{cs} = 2 \frac{B_e}{B_{cs}} \frac{S_d}{(D_{ext} - D_{int})} \quad (10)$$

with B_{cr} and B_{cs} are the magnetic inductions in the rotor and stator yoke.

The magnet section is:

$$S_a = \frac{A_{dent}}{2} \left(\left(\frac{D_{ext}}{2} \right)^2 - \left(\frac{D_{int}}{2} \right)^2 \right) \quad (11)$$

The magnet volume is then:

$$V_a = E_a S_a \quad (12)$$

The magnet mass is given as follow:

$$M_a = V_a M_{va} \quad (13)$$

with M_{va} is the magnets density.

The stator yoke mass:

$$M_{cs} = M_{vt} \frac{\pi}{4} (D_{ext}^2 - D_{int}^2) H_{cs} \quad (14)$$

with M_{vt} is the steel sheets density.

The main teeth Mass:

$$M_d = M_{vt} N_d S_d H_e \quad (15)$$

4. Optimization of the airgap flux density

In axial flux machines, the airgap flux density is an important design parameter which has significant effect on the machine characteristics. Therefore, in order to optimize the machine performance, the airgap flux density must be chosen carefully [13].
Figure 6 shows the power density variation and the mass as a function of airgap flux density for the machine.

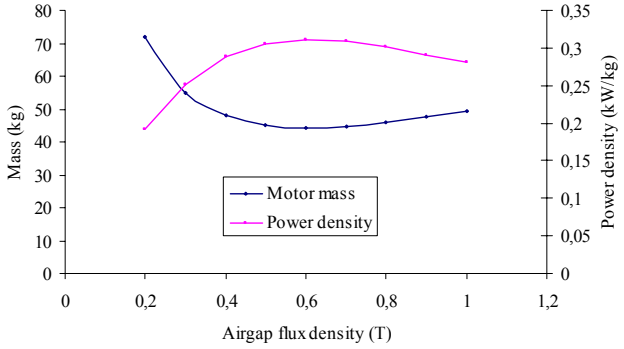

Figure 6: Power density and mass of machine vs. air-gap flux density

Figure 7 shows the efficiency variation as a function of airgap flux density for the machine.

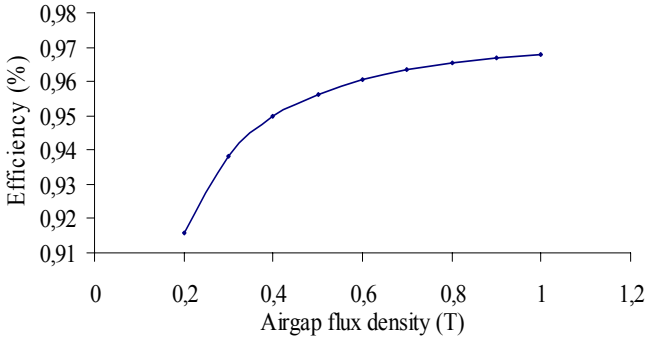

Figure7: Efficiency of machine vs. air-gap flux density

As can be seen from these figures, the maximum power density occurs at an airgap flux density of 0.6 T. For that maximum power density point, the machine efficiency is 96 %.

5. Optimization of the pole Number

The pole number was an important factor for the motor design. Using a higher pole number reduces the end winding length and the stator back thickness, but increases the fundamental frequency of the machine. A higher fundamental frequency gives higher iron losses and requires smaller strands in the wires to reduce the skin effect [14].

Figures 8, 9 and 10 represent respectively the total loss, machine efficiency and power density for different pole number.

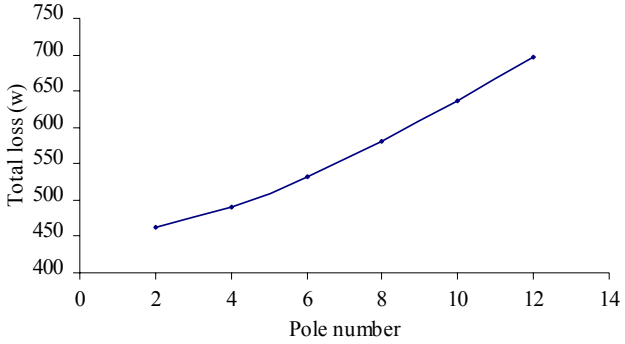

Figure 8: Total loss for different pole number

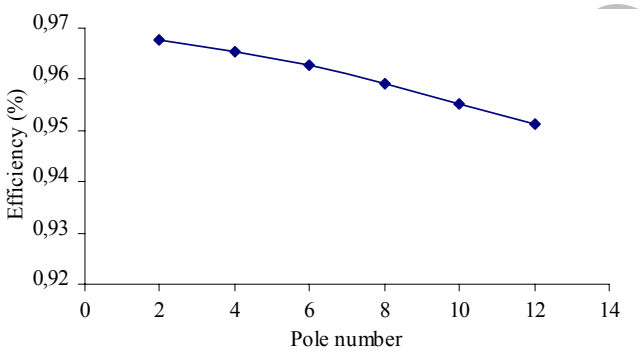

Figure 9: Machine efficiency for different pole number

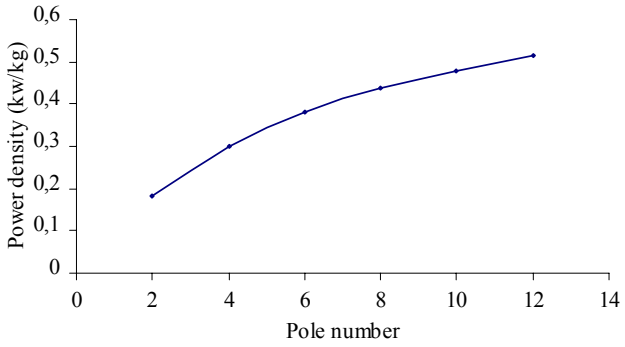

Figure10: Power density for different pole number

For the machine, a high pole number was preferred in order to minimize the effects of centrifugal forces on the end windings. Extremely high pole numbers are avoided because of the radial and axial space limitation of the motor and they give excessive leakage of magnet flux.

A reasonable pole number for the machine after optimization should be 8 or higher, the machine will not only have the maximum Power density but also will satisfy the loss and efficiency constraints [15].

After consideration of many alternatives, 8 poles were chosen which corresponds to an output frequency of 163 Hz when the motor speed is 2450 rev/min.

6. Finite Elements Analysis

Having completed the design process, the finite elements method is employed to analyze the magnetic field distribution of the proposed machine.

A two-dimensional finite elements analysis aoftware, Maxwell© 2D, was used in the analyses.

By fixing the magnet position into an appropriate parameter it is possible to rotate the rotor with discrete steps and solve a set of magneto static problems in order to detect the emf waveform and the waveform of torque as a function of the rotor position.

The magnetic field distributions of the machine at different load conditions and rotor position angles are analyzed.

In order to model the rotor rotation, the airgap is defined with a sliding surface splitting the airgap into two layers. One of these layers is fixed to the rotor while the other one is fixed to the stator [16].

A. Magnetic field

The positional variation of the magnetic field distribution at no load corresponding to 0 and 23 mechanical degrees of rotor rotation is seen in figures 11 and 12 as representative examples.

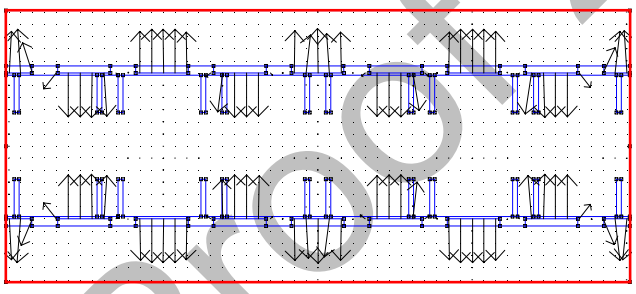

Figure11: Magnetic field direction

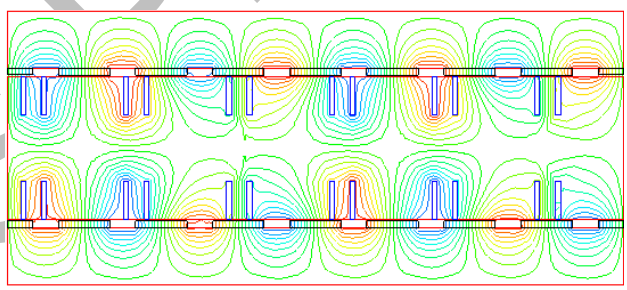

Figure12: Magnetic field distributions

For different positions of the rotor in versus the stator, the flux crossed by the machine winding is represented on the figures 13 and 14.

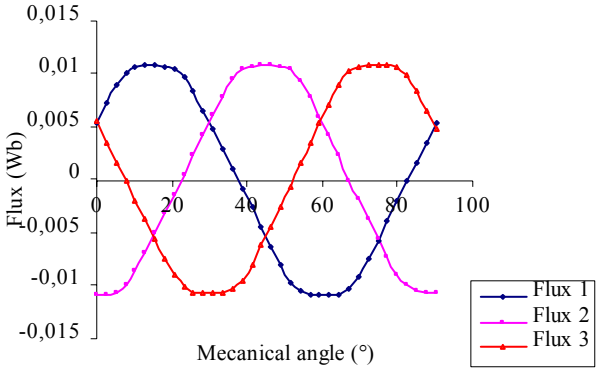

Figure13: Flux waveforms at no load

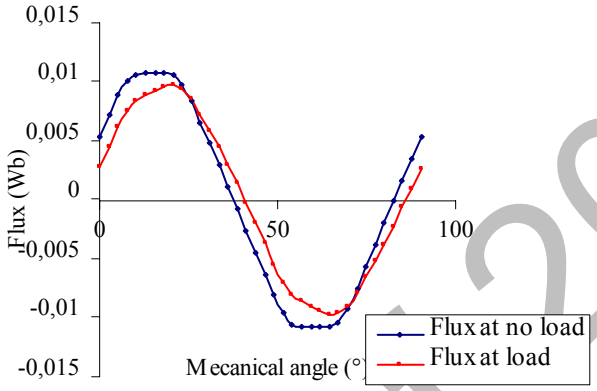

Figure 14: Flux through one phase at no load and at load

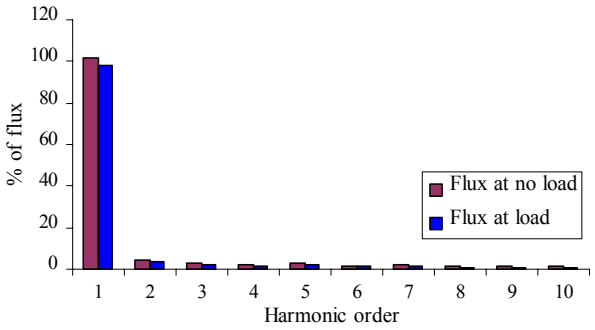

Figure 15: Flux harmonic spectrum

A comparison of the values of the flux between the finite elements method (FEM) results and sizing analysis results is tabulated in table 2. From the no load and load airgap flux plots and the table, it is seen that the results agree well.

TABLE 2: Flux comparison

	Analytic	FEM
Flux at no load	0,012	0,011
Flux at load	0,01	0,009

B. flux density

The value of the flux density in various machine parts is an important variable in the design of permanent magnet motors. It is the determining parameter in both core losses and the amount of saturation to which the machine is exposed. The exposure of the varying flux density at various machine parts is studied with the use of electromotive force [17].

In figure 16, flux density distributions at no load are shown. It is clearly seen that the flux density values at different cross-sections of the machine are not equal.

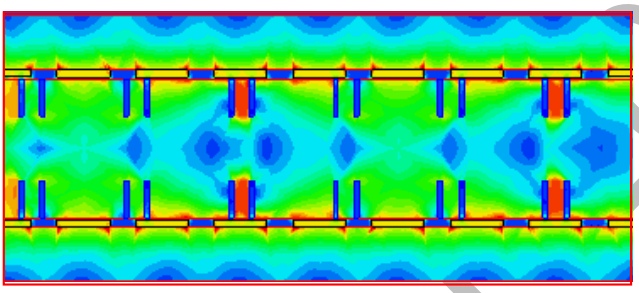

Figure 16: Flux density distributions at no load

Figure 17 shows the airgap flux density waveform over a two pole cross-section in mechanical degrees at no-load, the discontinuities due to slotting.

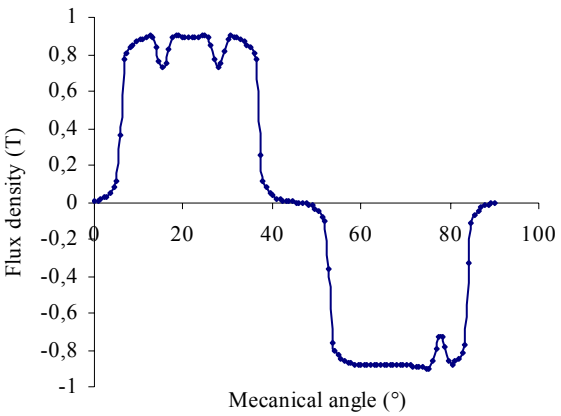

Figure 17: Airgap flux density waveforms at no-load

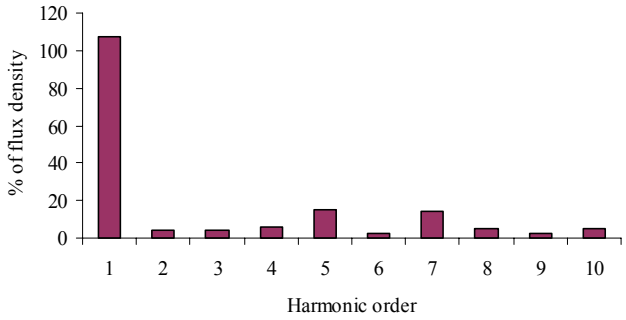

Figure18: Harmonic spectrum of flux density

The motor have substantial 5th and 7th airgap flux density harmonics, as shown in figure 18, and they are 14,78% and 14,61% of the fundamental component of 0,8 T respectively.

C. Electromotive force

Finite elements analysis conducted at incremental rotor positions are also used to calculate the phase-emf waveforms. The curves are deduced from the time derivative of the obtained flux variation with respect to rotor position.

$$e = -N_{sph}.\frac{d\Phi}{dt} \tag{16}$$

where Φ is the coil flux obtained from 2D finite elements method.

The time step Δt is proportional to the change of rotor angular position between computation points at known rotor angular speed [18].

Figures 19 and 20 show the EMF waveforms at no load and at load.

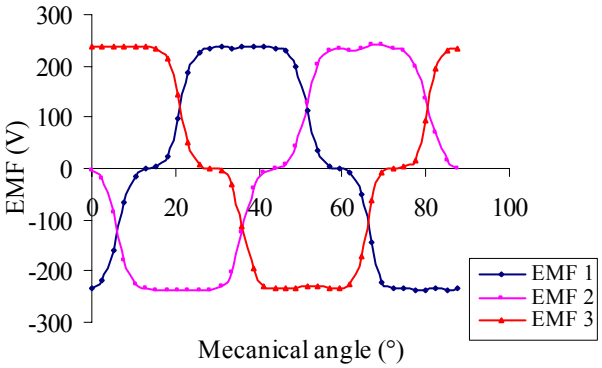

Figure 19: Electromotive forces at no load

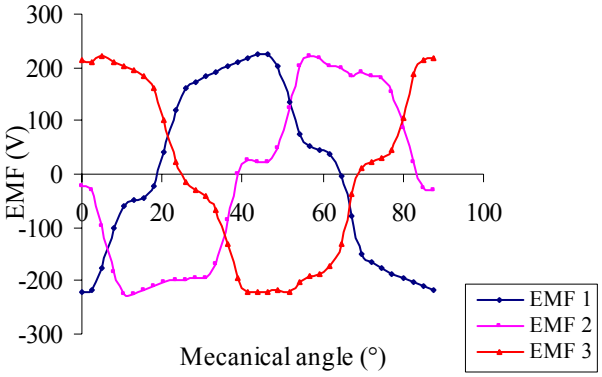

Figure 20: Electromotive forces at load

The figure 21 shows the EMF harmonic spectrum at no load and at load.

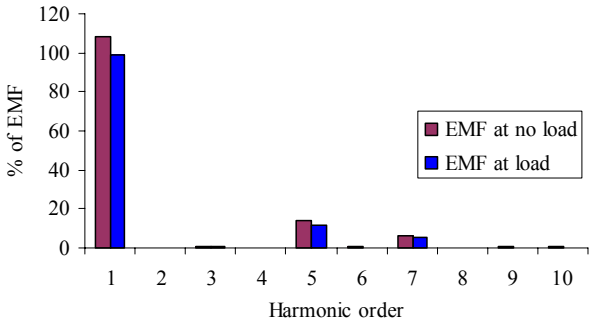

Figure 21: EMF harmonic spectrum

These figures show the harmonics and potential asymmetries, though for the EMF at load, the deformation at the bearing level is due to leakage flux variable in function to the angular position of the rotor.

The EMF at no load shows some harmonics and very slight imbalance. The motor have substantial 5^{th} and 7^{th} EMF harmonics, the total harmonic distortion (THD) content of EMF at no load and at load is 14,8% and 13,61% respectively

D. Machine torque

One important advantage of using finite elements analysis in machine design is the ability to calculate the torque variations such as cogging torque, ripple torque and total torque with changes in rotor position [19]. Figures 22 and 23 show respectively the total torque and the torque harmonic spectrum of the machine.

Ripple torque is mainly due to the fluctuations of the field distribution and the armature magneto motive force which depends on the motor magnetic structure and the armature current waveform. Despite the fact that these torque components add unwanted harmonics to the pulsating torque, there exist certain techniques to minimize both cogging torque and ripple torque components of these disc type machines.

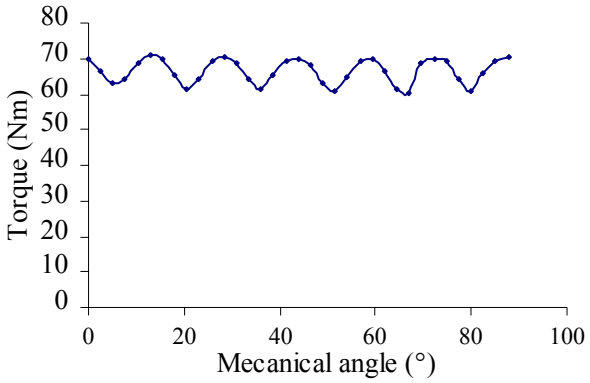

Figure 22: Torque with respect to rotor position.

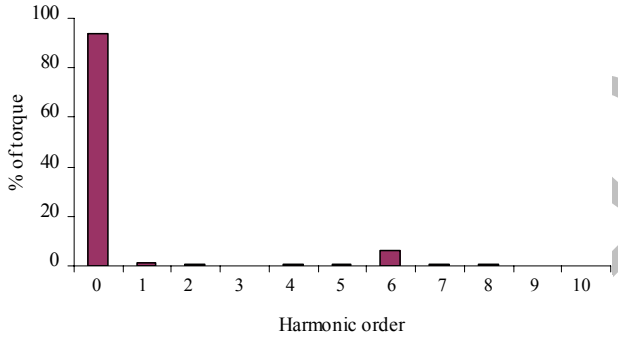

Figure 23: Torque harmonic spectrum

E. Cogging torque

In general, the total torque of a permanent magnet machine has three torque components: average torque, ripple torque and cogging torque.
Cogging torque occurs due to the reluctance variations in the airgap mainly because of slotting. This component also exists when there is no armature excitation, so it can be determined with the FE method by calculating the torque for several positions of the rotor at no-load [20]. The results are presented in figure 24.

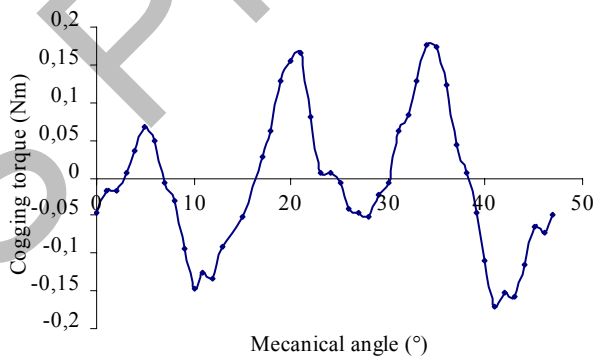

Figure 24: Cogging torque

7. Conclusion

A modular axial flux surface mounted permanent magnet machine has been presented in this paper.

First, the machine structure and principles were illustrated. An analytical sizing using generalized sizing equations was introduced in the second section. Finite elements models have been developed to yield reasonable predictions of the torque quality, flux density and field distribution of the motor.

According to finite elements method computations, the proposed magnet design produces an almost sinusoidal emf waveform.

Finally this machine could be a potential candidate in many cases, especially suitable for cases where an outside rotor is preferred, such as electric automobile motors

References

[1] S. Tounsi, F. Gillon, S. Brisset, P. Brochet, R. Neji, "Design of an axial flux brushless DC motor for electric vehicle", ICEM2002 CD: ICEM02-581.

[2] Y. Liao, F. Liang, T. A. Lipo, "A novel permanent magnet motor with doubly salient structure", in Conf. Rec. IEEE-IAS Annu. Meeting, vol. 1, Houston, TX, 1992, pp. 308–316.

[3] D. Qin, R. Qu, T. A. Lipo, "A novel electric machine employing torque magnification and flux concentration effects", in Conf. Rec.IEEE-IAS Annu.Meeting,vol. 1, Phonix, AZ, 1999, pp. 132–139.

[4] F. Profumo, Z. Zhang, A. Tenconi, "Axial Flux Machines Drives: A New Viable Solution for Electric Cars", IEEE Transactions on Industrial Electronics, Vol. 44, pp. 39- 45, 1997.

[5] Z. Zhang, F. Profumo, A. Tenconi, "Design of an axial flux interior PM synchronous motor with a wide speed range", Proceedings of International Conference on Electrical Machines, Vol. III, pp. 273-278, 1996.

[6] S. Brisset, F. Gillon, P. Brochet, "Manufacturing cost reduction in brushless DC motors", ICEM2002 CD: ICEM02-546.

[7] S. Tounsi, R. Neji, M. Gzara, F. Sellami, "Cost reduction of permanent magnet synchronous motor with axial flux". ICEM-04 (16th International Conference on Electrical Machines), 5-8 September, Cracow-Poland.

[8] A. Parviainen, J. Pyrhönen, M. Niemelä, "Axial flux interior permanent magnet synchronous motor with sinusoidally shaped magnets", ISEF 2001-10th International Symposium on Electromagnetic Fields in Electrical Engineering.

[9] M. Lajoie-Mazenc, B. Nogarede, and J. C. Fagundes, "Analysis of torque ripple in electronically commutated permanent magnet machines and minimization methods",in Proc. Inst. Elect. Eng. Conf. Publ., 1989, pp. 85–89.

[10] Y. D. Chun, J. Lee, and S.Wakao, "Overhang effect analysis of brushless DC motor by 3D equivalent magnetic circuit network method", IEEE Trans. Magn., vol. 39, no. 3, pp. 1610–1613, May 2003.

[11] X. Kestelyn, E.Semail, D.Loriol, "Direct torque control of a multi-phase permanent magnet synchronous motor drive", Application to a Five-phase One IEMDC 2005 de San Antonio

[12] J. Ha,K. Ide, T. Sawa, S. Sul, "Sensorless position control and initial position estimation of an interior permanent magnet motor", Thirty-Sixth IAS Annual Meeting Conference Record of the 2001 IEEE

[13] E. Nordlund, S. Tsakok, "Lumped circuit model of an axial flux motor", Published in the Proceedings of the 21st Worldwide Battery, Hybrid and Fuel Cell Electric Vehicle Symposium & Exhibition, EVS-21, Monaco, 2-6 April, 2005.

[14] J. F. Gieras, "Analytical approach to cogging torque calculation of PM brushless motors", IEEE Transactions on Industry Applications, Vol 40, No 5 September/ October 2004.

[15] M. S. Islam, S. Mir, T. Sebastian, "Issues in reducing the cogging torque of mass-produced permanent-magnet brushless DC motor", IEEE Transactions on Industry Applications, Vol 40, No 3 May/June 2004.

[16] E.Nordlund, "Simulation and design of a radial-radial four-quadrant transducer for hybrid vehicles", licentiate thesis presented in Feb 2003 at Royal institute of Technology, KTH, Stockholm.

[17] Brushless Permanent Magnet Motor Tutorial, Flux 2D version 7.5, Cedrat, March 2001.

[18] P. Thelin, J. Soulard, H.-P. Nee, C. Sadarangani, "Comparison between different ways to calculate the induced no-load voltage of PM synchronous motors using finite element methods", 4th International Conference on Power Electronics & Drive System, 2001, PEDS´01, Bali, Indonesia.

[19] D. Vizireanu, S. Brisset, X. Kestelyn, P. Brochet, Y. Milet, D. Laloy, "Polyphased Modular Direct-Drive Wind Turbine Generator", EPE 05.

[20] S. Salon, K. Sivasubramaniam, L. Tukenmez-Ergene, "An approach for determining the source of torque harmonics in brushless dc motors", in Proc. Int. Conf. Elect. Mach., vol. 3, Espoo, Finland, Aug. 2000, pp. 1707–1711.